

High Quality Dispersions of Hexabenzocoronene in Organic Solvents

J. Marguerite Hughes,[†] Yenny Hernandez,[‡] Damian Aherne,[†] Lukas Doessel,[‡] Klaus Müllen,[‡] Ben Moreton,[§] Thomas W. White,[§] Cerianne Partridge,[§] Giovanni Costantini,[§] Aleksey Shmeliov,[⊥] Mervyn Shannon,[¶] Valeria Nicolosi,^{†,#} and Jonathan N Coleman^{*,†}

[†]School of Physics & CRANN, Trinity College Dublin, University of Dublin, Dublin 2, Ireland

[‡]The Max Planck Institute for Polymer Research, D-55128 Mainz, Germany

[§]Department of Chemistry, University of Warwick, Coventry CV4 7AL, U.K.

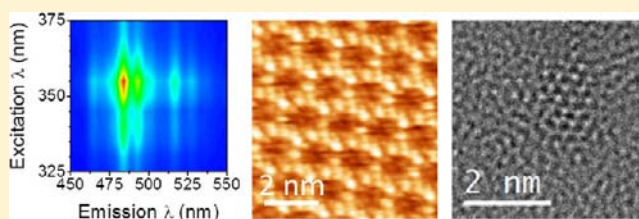
[⊥]Department of Materials, University of Oxford, Parks Road, Oxford OX1 3PH, U.K.

[¶]SuperSTEM, STFC Daresbury Laboratories, Keckwick Lane, Warrington, WA4 4AD, U.K.

[#]Schools of Chemistry and Physics & CRANN, Trinity College Dublin, University of Dublin, Dublin 2, Ireland

S Supporting Information

ABSTRACT: We have studied the exfoliation and dispersion of hexabenzocoronene (HBC) in 28 different solvents. We see a wide range of dispersed concentrations and aggregation states, all of which can be related to the solvent properties. To a first approximation, the dispersed concentration is maximized for solvents with Hildebrand solubility parameter close to $21 \text{ MPa}^{1/2}$, similar to graphitic materials such as nanotubes and graphene. We have also studied the concentration dependence of the absorbance and photoluminescence of HBC for both a good solvent, cyclohexyl pyrrolidone (CHP), and a poor solvent, tetrahydrofuran (THF). In both cases, we observe features that can be associated with either individual molecules or aggregates, allowing us to establish metrics both for aggregate and individual molecule content. While the aggregate content always increases with concentration, good solvents disperse individual molecules at relatively high concentrations while poor solvents display aggregation even at low concentrations. Using these metrics, we determine that large populations of individual molecules are present at low concentrations in certain solvents with Hildebrand solubility parameters close to $21 \text{ MPa}^{1/2}$. However, the aggregation state of HBC is considerably more sensitive to solvent Hildebrand parameter for halogenated solvents than for amide solvents. We find a combination of high overall concentrations and large populations of individual molecules in four solvents: cyclohexyl pyrrolidone, 1-chloronaphthalene, 1-bromonaphthalene, and 1,2,4-trichlorobenzene. Scanning tunnelling microscopy (STM) measurements show the formation of self-assembled monolayers at the interface between a HBC–solvent dispersion and a highly oriented pyrolytic graphite (HOPG) substrate. Similar structures were observed on ultrathin supports by aberration-corrected transmission electron microscopy (TEM). Also observed were graphitic objects of size $\sim 1 \text{ nm}$ consistent with monomers or aggregated stacks of very few monomers. We believe this is strong evidence of the presence of individual molecules in dispersions prepared with appropriate solvents.



■ INTRODUCTION

Hexabenzocoronene (HBC) is an extended aromatic molecule with the chemical formula $\text{C}_{42}\text{H}_{18}$ (see inset in Figure 1), first studied by Erich Clar in 1959.¹ It has sustained much research interest in recent years, in areas from synthetic chemistry to astrophysics.^{2–6} One of the reasons for this interest is that HBC can be considered to be a prototype for large, planar hydrocarbons. To date, a variety of these have been prepared in forms ranging from flat triangular molecules ($\text{C}_{60}\text{H}_{24}$)⁷ to giant discotic molecules ($\text{C}_{222}\text{H}_{42}$).⁸ However, a major problem, common to all of these planar hydrocarbons, is that they are generally considered insoluble in common solvents. One way to address this problem is to attach alkyl chains around the periphery, rendering them soluble.^{6,9} This has been very successful; substituted HBC has been cast from solution into films for various applications, from thin film transistors^{10,11}

to heterojunction solar cells.^{12–14} It is probable, however, that the presence of the solubilizing substituent groups has considerable influence on the structure of such films. For example, in solar cells, the alkyl chains take up space that could otherwise be occupied by photoactive, semiconducting material. In addition, in films of columnar structures,^{11,14} the presence of side chains is likely to affect the packing of the discs within the columns. This may have negative consequences such as reduction in carrier mobility. Thus, the ability to solution process unsubstituted planar hydrocarbons such as HBC, $\text{C}_{60}\text{H}_{24}$, or $\text{C}_{222}\text{H}_{42}$ would be a great advantage.

It has recently been demonstrated that HBC can be dispersed to the level of single molecules in aqueous surfactant

Received: April 17, 2012

Published: June 20, 2012

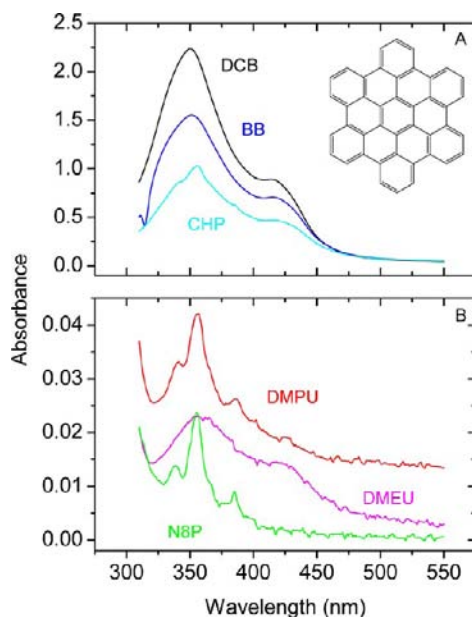


Figure 1. Selected absorption spectra for HBC dispersed in various solvents after centrifugation. For clarity, these have been separated into (A) highly absorbent dispersions (dichlorobenzene (DCB), benzyl benzoate (BB), and cyclohexyl pyrrolidone (CHP)) and (B) dispersions which display lower absorbance (*n*-octyl pyrrolidone (N8P), 1,3-dimethyl-2-imidazolidinone (DMEU), and 1,3-dimethyl-3,4,5,6-tetrahydro-2(1*H*)-pyrimidinone (DMPU)). The inset in panel A depicts the chemical structure of HBC.

solutions.¹⁵ While this is a great advance, it would be considerably more attractive to disperse HBC and similar molecules in appropriate solvents without the need for surfactant. Pure (unsubstituted) HBC has to date been dispersed in only one organic solvent (1,2,4-trichlorobenzene).^{1,16} It would be advantageous to extend significantly the number of good solvents for HBC and, in so doing, develop an understanding of the solution thermodynamics involved. We believe this can be achieved by utilizing recent advances in the exfoliation of the ultimate planar hydrocarbon: graphene.

A graphene sheet consists of an atomically thin array of sp^2 bonded carbon atoms organized in a planar hexagonal arrangement. Graphene has generated huge interest since early reports of its mechanical exfoliation^{17–19} and has the potential to be used in many applications. In many cases, such applications would require large quantities of exfoliated material, and so a great deal of work has been focused on the exfoliation of graphite using solvents to give graphene.^{20–27} It has become clear that sonication of graphite in solvents with solubility parameters in a certain range results in the production of large numbers of graphene flakes which are stabilized against re-aggregation by interactions with the solvent.²⁸ This method has two distinct advantages: it can potentially be scaled up and the graphene produced is relatively defect-free.²⁵

Because HBC can be considered a molecular analogue of graphene, there is much to be learned about its dispersion using solvents that have been employed to exfoliate graphene. One possibility is that HBC can be dispersed in the same set of solvents that are now routinely used to disperse graphene. This would imply that certain molecular properties of HBC, such as the presence of a hydrogen terminated molecular edge, play little or no role in the solvent–HBC interaction. This would be extremely interesting, as it would suggest that planar hydro-

carbons of all sizes can be dispersed in such solvents. Conversely, significant differences may be found between the sets of solvents which effectively disperse HBC and graphene. This would highlight the influence of the molecular edge, and other HBC-specific properties, on the solvation process.

It is also possible that studying the exfoliation and dispersion of HBC can in turn inform and improve the equivalent processes for graphene. While much work has been done to study graphene exfoliation, a number of problems remain. First, the exfoliation process requires protracted sonication to break up the graphitic crystallites.²⁵ It is difficult to be certain whether the dispersed concentration is controlled by solvent–graphene interactions or is limited by sonication effects. Second, it is difficult to determine the aggregation state of the exfoliated graphene. This is usually achieved by tedious TEM or AFM characterization.²⁵ If, however, it is found that the same solvents tend to exfoliate both HBC and graphene, HBC might be used as a proxy for graphene in dispersion studies. Compared to graphene, such a molecule would be easily dispersed because of its relatively small size, reducing the effect of sonication on the final dispersion. In addition, HBC is strongly photoluminescent,^{16,29} and both absorbance and photoluminescence have been shown to be sensitive to the aggregation state of the molecule.^{9,15} It is likely that some elements of its spectroscopic response could provide information about its aggregation state, allowing in situ measurements of dispersion quality. Thus, HBC could be used to screen new solvents or solvent blends for graphene in a relatively quick and efficient manner.

Overall, the identification of good solvents for HBC would yield several benefits. It would provide access to dispersed, exfoliated HBC for fundamental studies or for applications. More importantly, understanding the rules that determine what solvents can be used to disperse HBC would provide information on intermolecular interactions between HBC and other molecules and, hence, the interaction of other graphene-like materials with solvents. This knowledge could be directed to improve our ability to disperse and so process these materials. This is important, as HBC can be thought of as the building block for the bottom-up production of important structures such as graphene nanoribbons.³⁰

In this work we describe a method to disperse HBC in a range of solvents. We focus on solvents that have previously been reported to disperse graphene, nanotubes, and C_{60} . We show that dispersed HBC has a spectroscopic fingerprint which provides information about the aggregation state of the molecule. We use this to develop a metric for the relative population of individual molecules. This then allows us to demonstrate that HBC is exfoliated in solvents with particular values of Hildebrand solubility parameters. Scanning tunnelling microscopy (STM) is used as a further means to probe the HBC dispersion by analyzing the molecular self-assembly at the solid–liquid interface. The formation of single-molecule thick films for certain solvents supports the spectroscopic observations of their ability to efficiently disperse HBC. In addition, we have deposited dilute dispersions on ultrathin supports, and aberration-corrected high resolution transmission electron microscopy (HRTEM) and aberration-corrected scanning transmission electron microscopy (STEM) have been used to image structures similar to those observed using STM. In some cases, we also see well-defined, isolated objects of size ~ 1 nm that we identify as small cofacially stacked aggregates or perhaps individual HBC molecules.

RESULTS AND DISCUSSION

Saturated Dispersions of HBC. In this work, we study dispersions of HBC in 28 solvents (we use the term dispersion as we have no evidence as yet that the HBC–solvent mixtures form a thermodynamic solution.³¹ See the Experimental Methods section for a complete list of solvents and acronyms). The solvents can be roughly divided into three classes: halogenated aromatic solvents, amides and structurally similar solvents (such as γ -butyrolactone), and other common laboratory solvents, such as toluene. The halogenated aromatic solvents used were chosen on the basis that several of them were previously reported as excellent solvents for C_{60} ,³² while 1,2,4-trichlorobenzene has further been highlighted in the literature as a dispersant of HBC itself.^{1,16} The amide solvents were selected because of their good performance in dispersing both SWNTs and graphene.^{23,24,31} Finally, several common laboratory solvents were employed as a comparison to the first two groups, as they have appeared as such in other solubility studies.^{23,33}

Dispersions were prepared by sonication followed by centrifugation. We assume that the obtained concentration is the maximum allowed by the intrinsic intermolecular interactions between solvent and HBC. After centrifugation, absorbance spectra were recorded as illustrated in Figure 1. In general, the spectra were similar to those reported by Englert et al. for surfactant-stabilized HBC.¹⁵ For example, for those solvents with high HBC absorbance, broad absorbance spectra displaying two poorly resolved features at ~ 350 and ~ 421 nm were observed, in line with Englert's observations (e.g., DCB and benzyl benzoate (BB) in Figure 1A). These features have also been seen in substituted HBCs, and have been attributed to absorbance in the so-called Clar β and p bands, respectively.³⁴

However, some solvents, typically those with lower HBC absorbance, revealed significantly different spectral shapes. Figure 1B shows spectra for HBC in N8P and DMPU, which display sharp peaks at ~ 338 , ~ 356 , and ~ 386 nm. Other solvents which exhibited such features were NEP, NMP, and N12P. Interestingly, these are all solvents which tend to exfoliate nanotubes and graphene well.^{24,33} These features are among those previously assigned to specific β and p transitions observed in *individual* HBC molecules suspended in Ar and Ne and HBC dispersed in 1,2,4-trichlorobenzene; furthermore the spectra are very similar to excitation spectra (detected at 482 nm) measured for what appear to be unaggregated HBC molecules dispersed with the surfactant sodium dodecyl sulfate.^{1,2,4,15,16,35}

We can explain these observations by noting that high absorbance means high concentration as described by the Lambert–Beer law; moreover, molecular aggregation is more likely as concentration is increased.^{10,36–38} Considering these facts, the correlation between high absorbance values and spectral broadening observed for solvents such as DCB and BB suggests that such broadening can be explained by aggregation of HBC at high concentrations. As such, the spectral shape (the presence/absence of multiple peaks and the sharpness/broadening thereof) may be a measure of the aggregation state of the molecule, with sharp peaks indicating low aggregation.

However, it is worth noting that some high absorbance (and so we assume high concentration) dispersions display some remnant of the specific β and p peaks described above (Figure

1A, cyclohexyl pyrrolidone (CHP)) while some low absorbance (and so we assume low concentration) dispersions have broadened absorbance spectra (Figure 1B, DMEU). Thus there may be some decoupling between absolute absorbance and aggregation state, such that we do not always observe highly exfoliated molecules at low apparent concentrations and vice versa.

These variations in aggregation state between different solvents mean that the effective absorption coefficient will vary somewhat from solvent to solvent. This is because this coefficient contains contributions from both aggregates and individual molecules, species which do not necessarily have identical absorption coefficients. Their relative contributions depend on the aggregation state which in turn depends on the solvent. While this somewhat weakens the link between absolute absorbance and concentration, we can still use the measured absorbance as an approximate measure of dispersed concentration. This allows us to consider the properties of solvents which can be used to disperse HBC.

Standard solubility theory suggests that dissolution of a solute in a solvent is favorable when the enthalpy of mixing is low.³⁹ For a given solute–solvent combination, the enthalpy of mixing per volume of mixture is given by the Hildebrand–Scatchard expression, which can be written as^{31,39,40}

$$\Delta H_{\text{mix}}/V \approx (\delta_{T,A} - \delta_{T,B})^2 \phi(1 - \phi) \approx (\delta_{T,A} - \delta_{T,B})^2 \phi \quad (1)$$

where $\delta_{T,A}$ and $\delta_{T,B}$ are the Hildebrand solubility parameters of the solute and solvent, respectively, and ϕ is the solute volume fraction. The solute volume fraction is related to the dispersed concentration, C , by $C = \phi\rho$, where ρ is the solute mass density. We make the approximation that $(1 - \phi) \approx 1$, that is, that all dispersed concentrations are relatively low. We note that this expression strictly applies only to solutes with relatively low molecular weight. Macromolecular solutes such as polymers require an extra multiplicative constant of $2/3$ or $1/3$ depending on their dimensionality.⁴⁰

Equation 1 clearly shows that dispersion is favored when the solubility parameters of solvent and solute match. The Hildebrand solubility parameter of a material is the square root of the (total) cohesive energy density of the material and has been tabulated for a wide range of solvents.⁴¹ It can be shown that for a solvent and solute in thermodynamic equilibrium, the maximum dispersed concentration, C , is given by⁴²

$$C \propto \exp\left[-\frac{\bar{v}_A}{RT} \frac{\partial(\Delta H_{\text{mix}}/V)}{\partial\phi}\right] \quad (2)$$

where \bar{v}_A is the solute molar volume. Substituting eq 1 into eq 2 for the case of HBC shows the maximum concentration of dispersed HBC to be approximately described by

$$C \propto \exp\left[-\frac{\bar{v}_{\text{HBC}}}{RT} (\delta_{T,\text{HBC}} - \delta_{T,\text{sol}})^2\right] \quad (3)$$

This expression predicts that the concentration is controlled by the solvent solubility parameter, $\delta_{T,\text{sol}}$ and that the concentration should yield a Gaussian peak when plotted versus $\delta_{T,\text{sol}}$. The full width at half-maximum (fwhm) of this peak is controlled by the molecular volume of HBC: $\text{fwhm} \approx 1.6(RT/\bar{v}_{\text{HBC}})^{1/2}$.⁴² Given that the molecular weight of HBC is $M_w = 522$ g/mol and approximating the density of the HBC core as ~ 2000 kg/m³, we can predict the width of the Gaussian

described by eq 3 to be $\text{fwhm} \approx 4.8 \text{ MPa}^{1/2}$ at room temperature.

To test the applicability of solubility theory, we make the assumption that the concentration is roughly proportional to the absorbance. We plot the peak absorbance of each sample (i.e., at $\sim 355 \text{ nm}$, A_{355}) measured in a 1 mm cuvette as a function of the solvent's Hildebrand solubility parameter (Figure 2). A peak centred at $21\text{--}22 \text{ MPa}^{1/2}$ is indeed

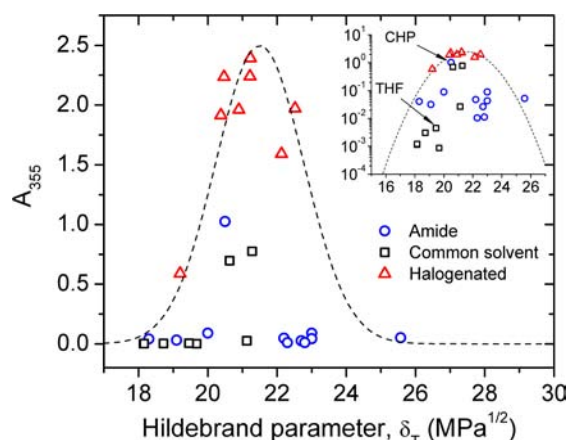


Figure 2. Absorbance of HBC solutions, measured at 355 nm, plotted as a function of the Hildebrand solubility parameter of the solvent. Inset: The same data on a semilogarithmic plot. The solvents are divided into amides, halogenated solvents, and common solvents. In both cases the dashed line is a Gaussian function. CHP and THF have been indicated by arrows.

observed. The data points within this peak can be bounded by a Gaussian envelope function (dashed line) centred at $\approx 21.5 \text{ MPa}^{1/2}$ and with full width at half maximum of $\approx 3 \text{ MPa}^{1/2}$. This implies that the Hildebrand parameter of HBC is $\delta_{T,\text{HBC}} \approx 21\text{--}22 \text{ MPa}^{1/2}$. This is comparable to other graphitic materials such as graphene, SWNT, and C_{60} , which have Hildebrand parameters of $\sim 21\text{--}22 \text{ MPa}^{1/2}$, $21 \text{ MPa}^{1/2}$, and $19.5 \text{ MPa}^{1/2}$, respectively.^{23,33,43} The experimental fwhm is also close to that predicted by eq 3.

It is worth noting, however, that the data in Figure 2 are rather scattered. The Gaussian curve is a very good envelope function—that is, it describes well the maximum observed concentration for a given Hildebrand parameter—still, many of the data points lie below it. There are probably two reasons for this. As described above, due to aggregation effects, it is likely that the effective absorption coefficient of HBC varies with solvent, introducing scatter into the graph. Second, Hildebrand solubility parameters are known to be imperfect, largely because they ignore nondispersive intermolecular interactions.³³ This generally results in solvents with concentrations below the Gaussian curve. This can be partially resolved by using Hansen solubility parameters (see the Supporting Information).^{41,44}

Dependence of Optical Spectra on Concentration: Aggregation Effects. It is clear from the above discussion that uncertainty about the relationship between aggregation and concentration is a significant problem. To resolve this issue it was decided to carry out a concentration study focusing on several solvents from the original experiment, whose post-centrifugation absorbances (1 mm cuvette) ranged from high (>1) to low (<0.01). A number of papers in the literature have previously reported a change in aggregation state with concentration which can be monitored using spectroscopic

methods.^{9,45} This would determine whether the spectral shapes were concentration-dependent, and whether a given shape could be attributed to a particular exfoliation state. If so, useful measures of dispersion effectiveness might be extracted.

For this study, the samples were prepared by bath sonicating HBC and solvent at 0.1 mg/mL for 2 h (these samples were not centrifuged, in order that the concentration would be known). Dilution series were then immediately prepared (concentration range $0.1\text{--}0.001 \text{ mg/mL}$), and each dilution was shaken vigorously before the next one was prepared. All samples then received a further 10 min sonication immediately prior to characterization. Absorbance measurements were taken in a 2 mm quartz cuvette.

Solvents investigated were 1-CN, CHP, DMPU, GBL, MB, and THF (in descending order of expected maximum solubility as per Figure 2). The dispersions were characterized at concentrations of 0.1, 0.05, 0.02, 0.01, 0.005, 0.002, and 0.001 mg/mL . Generally, the first three solvents exhibited similar behavior to one another, as did the latter three; therefore, complete results for CHP and THF (tetrahydrofuran) only will be included here.

Shown in Figure 3A are the normalized absorbance spectra for HBC–CHP at a range of concentrations. The lowest concentration spectrum is considerably different to the broadened HBC–CHP spectrum displayed in Figure 1A, instead resembling the spectra for DMPU and N8P seen in Figure 1B. As the concentration is increased, the bands at ~ 338 , ~ 356 , and $\sim 386 \text{ nm}$ broaden continuously; yet, even at 0.1 mg/mL , the remnants of these peaks are still observable. However, more interesting is the appearance and growth of a new feature at $\sim 421 \text{ nm}$. By 0.1 mg/mL , this feature has reached approximately half the intensity of the main peak and the spectrum resembles that presented in Figure 1A. It is worth noting that the transitions at ~ 338 , ~ 356 , and $\sim 386 \text{ nm}$ have been observed for individual HBC molecules in the gas phase (albeit shifted in accordance with environment) and appear to be intrinsic to the molecule.^{2,35} However, as the peak at 421 nm only appears with increasing concentration, we associate it with the presence of molecular aggregates. This assignment is supported by the fact that such a feature has been previously observed in absorption spectra of fluorenyl-HBC thin films but is absent in solution spectra of the same compounds.⁵ In addition, certain conjugated polymers are known to display absorbance peaks just below the band edge which have been associated with aggregation.^{36,46,47}

We can compare these results with those of HBC dispersed in THF as a function of concentration, as shown in Figure 3B. In the lowest concentration dispersion, the peaks at ~ 338 , ~ 356 , and $\sim 386 \text{ nm}$ are just visible. However, as the concentration increases, the main band undergoes substantial broadening such that the peaks at ~ 338 and $\sim 386 \text{ nm}$ cannot be seen for concentrations above 0.005 mg/mL . Moreover, in contrast to HBC–CHP, the feature at 421 nm is present even at the lowest concentration (0.001 mg/mL), increasing in intensity as the concentration is increased. These data emphasize the link between the presence of the 421 nm peak and spectral broadening, strongly supporting our suggestion as to its aggregate origin.

We can explore the role of concentration more fully by examining the concentration dependence of the photoluminescence of the dispersions just discussed. Shown in Figure 3C are photoluminescence emission spectra (excited at the main absorbance peak, $\sim 355 \text{ nm}$) for HBC–CHP,

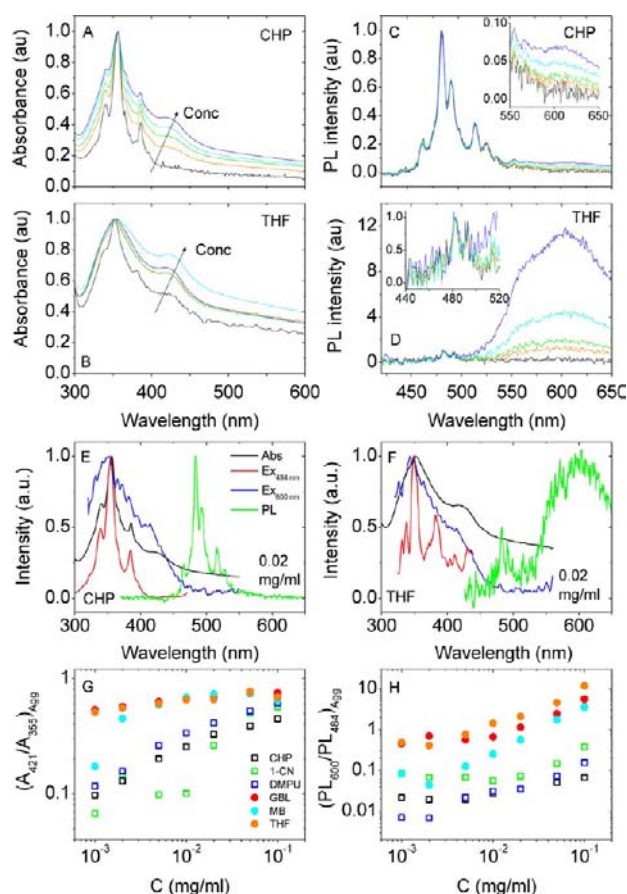


Figure 3. Concentration dependence of the optical properties of HBC dispersions. (A–B) Absorbance spectra for (A) HBC–CHP dispersions and (B) HBC–THF dispersions at a range of concentrations (0.002 to 0.1 mg/mL). (C–D) PL spectra measured for the same HBC–CHP (C) and HBC–THF (D) dispersions as in A and B. (E and F) Absorbance, PL and excitation spectra for HBC–CHP (E) and HBC–THF (F) dispersions at 0.02 mg/mL. In both cases, the excitation spectra were collected at two different emission wavelengths, 484 and 600 nm. (G) Ratio of absorbance at ~ 421 nm to that at ~ 355 nm taken from curves similar to those in panels A and C, but for a range of solvents, plotted as a function of HBC concentration. (H) Ratio of PL at ~ 600 nm to that at ~ 484 nm taken from curves similar to those in panels B and D, but for a range of solvents, plotted as a function of HBC concentration. The quantities in (G and H) are both metrics for the relative aggregate content.

normalized at 484 nm. The fine structure between ~ 450 and ~ 525 nm has previously been attributed to emission from individual HBC molecules, with the peak at ~ 464 nm associated with the optical gap of HBC.^{15,29,45} It is clear that the shape of the emission below ~ 530 nm does not change as the concentration increases. However, as the concentration is increased above ~ 0.02 mg/mL, the onset of broad, unstructured emission above 530 nm is observed (see inset). Such emission has been extensively reported for polycyclic hydrocarbons and ascribed to excimer formation within the dispersion.^{48,49} An excimer is defined as a dimer which is associated in an excited electronic state, but would dissociate in the absence of external restraints in its ground state.⁵⁰ In this sense, it differs from a true aggregate. However, the presence of this emission can also be linked to larger aggregate formation: for the HBC derivatives studied by Kastler et al.,⁴⁵ the relative intensity of the excimer peak as a function of concentration was

correlated with the NMR chemical shift with concentration, which was in turn a marker of self-aggregation beyond dimerization. Therefore, its intensity relative to the “monomer” emission peak (at ~ 484 nm) may be useful as a measure of aggregate formation.

DMPU and 1-chloronaphthalene (1-CN) produced similar results to CHP, although the fine structure of the HBC–1-chloronaphthalene sample was slightly less resolved than for CHP. Their characteristic “excimer” peaks were more pronounced, but also appeared at ~ 0.02 mg/mL.

The emission spectra for HBC–THF (normalized at ~ 483 nm) are displayed in Figure 3D. We can immediately see that even at low concentrations (~ 0.005 mg/mL) the “excimer” peak is already comparable in intensity to the 483 nm peak, suggesting that such dispersions are dominated by aggregates. For methyl benzoate and GBL, the broad emission becomes significant at higher concentrations than for THF (0.01 and 0.005 mg/mL, respectively) and does not achieve the same relative intensity at 0.1 mg/mL as it does in THF, but is still at least three times greater in magnitude than the 483 nm peak. The signal around 483 nm is also far less intense and less resolved in THF, MB, and GBL than in CHP. This is probably due to the better dispersion quality in CHP but may be partially attributed to lower quantum yields of HBC in the “poor” solvents.

To fully underline how these differences in spectral features differentiate good and bad solvents, we next inspect the photoluminescence excitation (PLE) spectra. Excitation spectra were taken for two different emission wavelengths, one corresponding to peak “individual” emission (~ 484 nm), the other to peak “excimer” emission (~ 600 nm), and compared to the shape of the absorption spectrum. Figure 3 panels E and F show absorbance, PL, and excitation spectra collected at 484 and 600 nm for both HBC–CHP and HBC–THF, respectively (0.02 mg/mL). In both cases, the same result is apparent. The excitation spectra collected at 484 nm, that is, in the region of the PL spectrum associated with individual molecule emission, resemble the absorbance spectra with sharp peaks observed at low concentrations. However, the excitation spectra collected at 600 nm, that is, in the region of the PL spectrum which we have shown to be associated with aggregated molecules, resemble the spectra containing broadened absorbance peaks observed at high concentrations. This is an important result as it clearly reveals a link between the sharp β and p bands in the absorption spectra and the sharp high energy region of the PL spectra. We associate these properties with individual molecules, noting that they occur most frequently at low concentrations. Equally important is the link between broadened absorption spectra, the feature at ~ 421 nm, and the broad low energy component of the PL spectra. We associate these properties with molecular aggregates, and note that they occur most frequently at higher concentrations. These results clearly show that certain distinct and well-defined regions of both absorbance and photoluminescence spectra contain information about individual and aggregated molecules. This allows us to use these spectra to study the relative populations of individual and aggregated HBC molecules as a function of concentration and solvent type.

From these results, we propose two metrics for aggregation. The first is the ratio of the secondary absorbance peak at ~ 421 nm (associated with the presence of aggregates) to the main absorbance peak at ~ 355 nm (associated with the presence of exfoliated molecules), or $(A_{421}/A_{355})_{\text{agg}}$. We include the

subscript “Agg” to emphasize that this quantity reflects the relative aggregate content. Plotted in Figure 3G is $(A_{421}/A_{355})_{\text{Agg}}$ as a function of concentration (log–log scale) for the six solvents studied. A clear demarcation between the three “good” and “bad” solvents at all concentrations can be identified: a high value of $(A_{421}/A_{355})_{\text{Agg}}$ at all concentrations is characteristic of poor solvents while a slow increase of $(A_{421}/A_{355})_{\text{Agg}}$ with increasing concentration is associated with good solvents. For clarity, good solvents are represented by open squares while poor solvents are shown as filled circles. We note that this metric has some limitations, as discussed in the SI.

As a second measure of aggregation, we suggest the ratio of the PL intensity for the excimer peak close to 600 nm to the intensity of the main peak at ~ 484 nm. This ratio, $(\text{PL}_{600}/\text{PL}_{484})_{\text{Agg}}$ is plotted against concentration for all six solvents in Figure 3H. In all cases, $(\text{PL}_{600}/\text{PL}_{484})_{\text{Agg}}$ increases steadily with concentration but is almost always larger for the “bad” solvents than for the good ones.

Such concentration-dependent aggregation affects are consistent with the presence of an individual–aggregate dynamic equilibrium. At low concentrations, the individual/aggregate distribution is dominated by individual HBC molecules while as the concentration is increased, the equilibrium shifts toward the aggregated state. Such behavior has been observed for a number of planar aromatic molecules including HBC derivatives.^{37,38,45} In our case, taking the 1-CN data as an example, it is clear from Figures 3G and H that significant aggregation begins to occur as the concentration is increased past $\approx 10^{-2}$ mg/mL. For HBC ($M_w = 522$ g/mol) this concentration is equivalent to $\approx 2 \times 10^{-5}$ M. Previous works on solutions of substituted HBCs have used proton NMR to monitor the aggregation state as a function of concentration.^{37,45} Such data have shown the onset of aggregation to occur at concentrations between 10^{-6} and 10^{-4} M depending on substituent group and solvent. This agreement confirms that the dispersion of unsubstituted HBC in appropriate solvents is at least as good at suppressing aggregation as functionalisation of the HBC core with bulky sidechains.

We can illustrate the solvent-dependent aggregation results more clearly using photoluminescence excitation–emission maps. The data in Figure 3H suggest CHP to be a particularly good solvent, methyl benzoate to be a mediocre solvent, and THF to be a particularly poor solvent. Shown in Figure 4 are excitation–emission maps for HBC at 0.02 mg/mL in CHP (A), methyl benzoate (B), and THF (C). It can clearly be seen that most of the emission in HBC–CHP is localized in a region of the map with emission wavelength close to $\lambda_{\text{em}} \approx 490$ nm for excitation wavelengths around $\lambda_{\text{ex}} \approx 350$ nm. This is exactly as would be expected for a sample containing predominately individual molecules. For HBC in methyl benzoate however, while some emission is observed in this region ($\lambda_{\text{em}} \sim 490$ nm, $\lambda_{\text{ex}} \sim 350$ nm), a large proportion of the light output comes from a broad region of the map with $\lambda_{\text{em}} > 550$ nm and $\lambda_{\text{ex}} \sim 320$ –420 nm. This is consistent with emission from both individuals and aggregates. In contrast, the HBC–THF spectrum is dominated primarily by aggregate emission ($\lambda_{\text{em}} > 550$ nm, $\lambda_{\text{ex}} \approx 320$ –420 nm).

Comparing Dispersions at a Common Concentration.

The previous section makes it clear that aggregation effects are present for all solvents but to a differing extent at different concentrations. We can separate the solvent dependence from the concentration dependence by preparing dispersions of HBC in all 28 solvents at the same concentration. To do this,

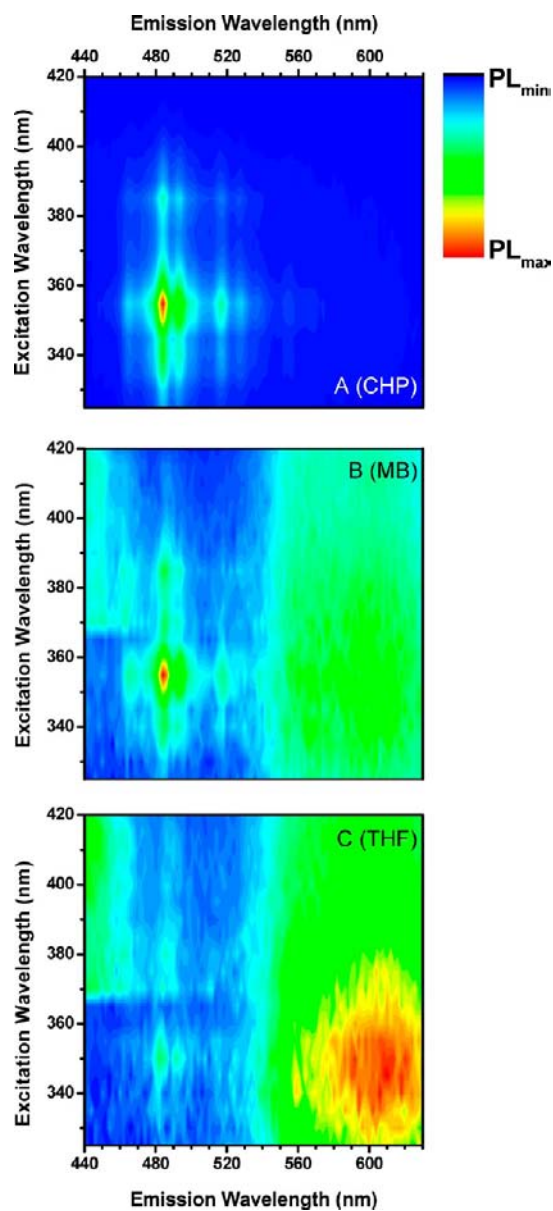


Figure 4. Excitation–emission maps for (A) HBC in cyclohexyl pyrrolidone (CHP); (B) HBC in methyl benzoate (MB); and (C) HBC in tetrahydrofuran (THF) at 0.02 mg/mL, measured with an emission slit width of 5 nm.

samples were prepared at 0.1 mg/mL as described previously, but then diluted to 0.002 mg/mL. They then received 10 min sonication after which absorption and PL spectra were collected. This concentration was chosen partly based on the fact that it minimized the PL signal from aggregates compared to individuals and assured the presence of individual molecules even in poor solvents. Moreover, it was dilute enough that inner filter and reabsorption effects were minimal.³⁶

In all cases the spectra were similar in form to those in Figure 3. It was clear from these spectra that all solvents contained both aggregates and individuals in varying ratios. In this work, we are particularly interested in understanding which solvents lead to high quality dispersions of HBC, which in effect means highly exfoliated dispersions, that is, those with a high proportion of individual HBC molecules. A suitable quantity to describe this is the ratio of the main absorbance peak to the low energy “aggregate” peak. This ratio will be large when the

aggregate population is low, that is, when the individual population is high. We denote this ratio $(A_{355}/A_{421})_{\text{Ind}}$ (as opposed to $(A_{421}/A_{355})_{\text{Agg}}$ seen earlier). To see the effect of solvent on the HBC exfoliation state, we plotted $(A_{355}/A_{421})_{\text{Ind}}$ as a function of Hildebrand solubility parameter, shown in Figure 5A. The data behave similarly overall to those shown in

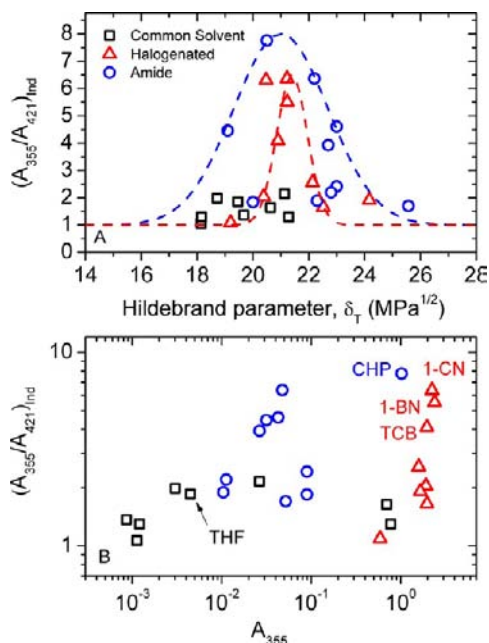


Figure 5. Dependence of relative monomer concentration on solvent solubility parameter and the total dispersed concentration. The relative content of individual, unaggregated HBC molecules (monomers) in the dispersion can be represented by the ratio of absorbance at ~ 355 nm to that at ~ 421 nm; $(A_{355}/A_{421})_{\text{Ind}}$. (A) This ratio is plotted as a function of the solvent Hildebrand solubility parameter. This data shows that the content of individual molecules is maximized for solvents with solubility parameters close to $21 \text{ MPa}^{1/2}$. The dashed lines in panel A are Gaussian curves as suggested by eq 3. We note that unlike the specific case described by eq 3, it is appropriate for the curves in Figure 5A to have an offset. This is because the ratio $(A_{355}/A_{421})_{\text{Ind}}$ will not be zero even for a very bad solvent. (B) The relative monomer content plotted versus the absolute absorbance of a saturated HBC dispersion (measured at 355 nm in a 1 mm cuvette), A_{355} . Here, A_{355} is an approximate measure of the maximum concentration achievable. Generally, the best solvents are those which disperse large amounts of HBC with high monomer content and can be found at the top right of the graph. Conversely, poor solvents appear at the bottom left. The best solvents are labeled: 1,2,4-trichlorobenzene (TCB), 1-chloronaphthalene (1-CN), 1-bromonaphthalene (1-BN), and cyclohexyl pyrrolidone (CHP). In addition, THF, as an example of a poor solvent, is also labeled. The data in this Figure is summarized in the Supporting Information, Table S1.

Figure 2, with a well-defined peak centered at $20\text{--}21 \text{ MPa}^{1/2}$. With the exception of the “common solvent” data, which shows no clear peak, the scatter appears to be reduced from that in Figure 2, indicating that $(A_{355}/A_{421})_{\text{Ind}}$ is a suitable measure of dispersion quality. In fact, the data for the amide solvents can be fitted with a Gaussian peak (by analogy with eq 3) centered at $21.0 \text{ MPa}^{1/2}$ and with a fwhm of $4 \text{ MPa}^{1/2}$. As above, this center position is consistent with graphitic carbons^{28,44} while the width is as expected for HBC (by eq 3). Yet, it is clear from the same data that the halogenated solvents also display a distinct narrow peak, this one centered at $21.4 \text{ MPa}^{1/2}$ and with

fwhm = $1.3 \text{ MPa}^{1/2}$. The narrowness of this peak indicates that the quality of HBC–halogenated solvent dispersions is much more sensitive to the detailed structure of the solvent than is the case for amide solvents. It is unclear why this should be. Equation 3 suggests that such narrowing is indicative of an increase in the molar volume of the dispersed species, that is, aggregation. However, the high values of $(A_{355}/A_{421})_{\text{Ind}}$ suggest these dispersions to be dominated by individual molecules. Alternatively, we have recently shown that surface entropy (solvation) effects can result in broadening of concentration–solubility parameter peaks relative to the value predicted by eq 3—but as yet we know of no mechanism which can result in such narrowing.⁴²

We remark here that to gain further understanding of the interactions controlling HBC dispersion, $(A_{355}/A_{421})_{\text{Ind}}$ may also be plotted against the individual Hansen solubility parameters (i.e., the dispersive, polar and hydrogen bonding components. See SI for details).^{23,33,41,51} Similar to Figure 5A, we find that $(A_{355}/A_{421})_{\text{Ind}}$ peaks for certain values of the three types of Hansen parameter. We estimate the dispersive, polar, and hydrogen bonding Hansen solubility parameters of HBC to be: $\delta_D = 18.5 \text{ MPa}^{1/2}$, $\delta_P = 7.5 \text{ MPa}^{1/2}$, and $\delta_H = 6 \text{ MPa}^{1/2}$. These are remarkably close to those values observed for successful carbon nanotube and graphene dispersants.^{23,33} This similarity suggests that solvation effects are dominated by HBC–solvent interactions at the basal plane rather than at the hydrogen-terminated edge. This therefore implies that the dispersion mechanism is similar for the wider family of graphitic materials of all sizes—in turn validating our choice of HBC as a model molecule for studying graphene dispersion in solvents.

In addition, knowledge of the Hansen parameters of HBC allows us to comment on the poor performance of the common lab solvents. None of the common solvents used in this study had all three Hansen parameters within $1 \text{ MPa}^{1/2}$ of those of HBC. This may partially explain the poor performance of these solvents. The common solvent with Hansen parameters closest to HBC (MB) was also the solvent with highest $(A_{355}/A_{421})_{\text{Ind}}$. This suggests that if a common lab solvent with the correct Hansen parameters could be found, it might perform relatively well. We had planned to identify a nonamide, nonhalogenated common solvent with the correct Hansen parameters to test its ability to exfoliate HBC. However, even using Hansen’s database (www.hansen-solubility.com), we could find no such solvent with all parameters within $1 \text{ MPa}^{1/2}$ of those of HBC.

Ideally, we would like to identify solvents that can disperse HBC at high concentration and achieve relatively good exfoliation. To test this, we plot $(A_{355}/A_{421})_{\text{Ind}}$ (all measured at 0.002 mg/mL) against our approximate metric for maximum achievable concentration, A_{355} , measured for centrifuged dispersions (as in Figure 2). In such a plot, the best solvents would be found at the top right, while poor solvents would appear at the bottom left. This data is shown in Figure 5B and shows a general correlation between exfoliation state ($(A_{355}/A_{421})_{\text{Ind}}$) and maximum concentration (A_{355}) for both amide and halogenated solvents. This is unsurprising as a successful solvent would be expected to produce both high concentrations and large quantities of individual molecules. It is worth noting that the data for the halogenated solvents is shifted to the right relative to the amide solvent data. This shows that halogenated solvents can produce high degrees of exfoliation, even at relatively high concentration. We note that four solvents yield particularly well-exfoliated, high concentration dispersions. These are CHP, 1-chloronaphthalene, 1-bromonaphthalene,

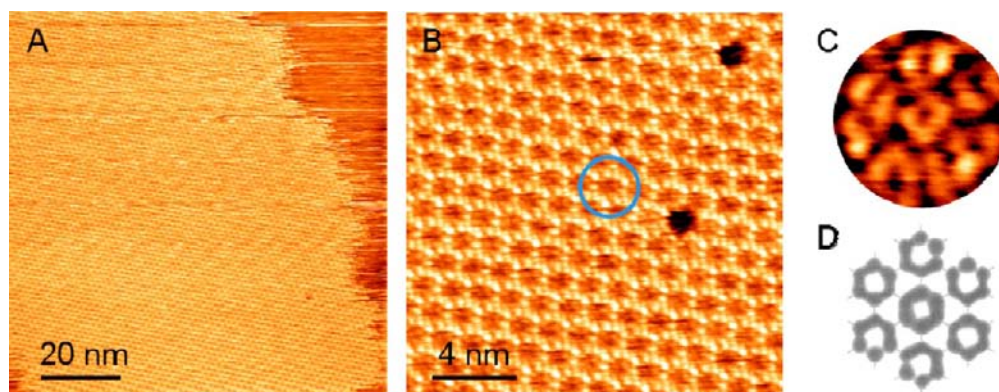


Figure 6. STM images of HBC in 1,2,4-trichlorobenzene on HOPG. (A) Molecular island of HBC ($V = -980$ mV, $I = 280$ pA). (B) Drift-corrected image showing molecular packing of HBC and lattice vacancies; the blue circle highlights an individual HBC molecule ($V = -980$ mV, $I = 280$ pA). (C) Drift-corrected single HBC molecule with submolecular resolution ($V = -390$ mV, $I = 390$ pA). (D) Calculated HOMO electron density of HBC (adapted from ref 54).

and 1,2,4-trichlorobenzene. It is known that CHP is an excellent dispersant for both nanotubes and graphene.^{23,33} These data suggest that the other solvents may also be promising candidates for exfoliating nanomaterials.

We note that the same analysis can be performed using a PL-based quantity reflecting the relative population of individual molecules, $(PL_{484}/PL_{600})_{\text{ind}}$. This is outlined in the Supporting Information.

Investigating Molecular Self-Assembly at the Solid/Liquid Interface. To further study the effect of the solvent on aggregation, the self-assembly of HBC at the solid–liquid interface has been investigated. Scanning tunnelling microscopy (STM) is an ideal characterization technique, due to its ability to produce highly resolved images of the interfacial structures formed when molecule-containing dispersions are brought into contact with conductive solid substrates.⁵³ The aromatic character of HBC suggests a strong adsorption on the highly oriented pyrolytic graphite (HOPG) substrates used here. However, the nature of the STM experiment imparts strict limitations on the solvents used: they must be sufficiently apolar, have a low volatility, and should wet the substrate well. As a result, not all of the solvents investigated spectroscopically here, such as fluorobenzene (too volatile) and CHP (too polar), were suitable for use in STM.

Three solvents with varying dispersion efficiencies were found to be appropriate for STM imaging: 1,2,4-trichlorobenzene, 2-BOEA, and CHB. Only deposition from 1,2,4-trichlorobenzene was successful, while multiple attempts using 2-BOEA and CHB found only bare HOPG, strongly suggesting no deposition was occurring.

Figure 6 shows typical STM images of the supramolecular layer formed from a dispersion of HBC at ~ 0.005 mg/mL in 1,2,4-trichlorobenzene. (All other samples for STM were prepared by directly dispersing HBC at 0.1 mg/mL in the solvent of interest, before sonicating and diluting as appropriate.) Figure 6A shows a large island with a periodic internal structure, attributed to individual HBC molecules. Surrounding this island is a darker, flat region assigned to bare HOPG. The borders of the HBC island are streaky along the scanning direction, caused by tip-dragging or thermally induced movements of the HBC molecules at the island's edges.

Shown in Figure 6B is a zoomed-in image of the molecular arrangement within the islands, where the single molecules are clearly visible (highlighted by a blue circle) as circular

depressions surrounded by a brighter ring. The darker spots in the right-hand side of Figure 6B are attributed to vacancies in the supramolecular layer. The periodicity and orientation of the molecules match that of the HBC monolayer previously identified in both vacuum and solution.^{52,54} When scanning with a negative bias (i.e., electrons tunnelling from filled molecular states to unfilled tip states) certain tip conditions result in the resolution of the intramolecular structure within the HBC molecules (Figure 6C). These images have a strong resemblance to the calculated spatial distribution of the HBC HOMO, as shown in Figure 6D.⁵⁴

Previous work on HBC depositions on HOPG in both vacuum⁵⁴ and solution⁵² showed that adsorption results in a planar and compact hexagonal HBC structure. In solution, where the amount deposited can be difficult to control, an organized second layer on top of this monolayer was also reported.⁵² However, during our investigation no evidence of this bilayer was ever observed, irrespective of the tunnelling parameters used or of the HBC concentration up to values of ~ 0.1 mg/mL. It is worth noting that the ability to image the spatial characteristics of the HBC HOMO is not proof of the existence of a second layer, as suggested in ref 52. While this might be the case for the adsorption on metals due to a strong molecule–substrate electronic coupling, this is not true for HOPG where the coupling is much weaker, meaning that such observations should be relatively routine.⁵⁵ It could therefore be suggested that the double layer structure observed by Samorí et al.⁵² only forms when the first layer is fully completed; a situation we were unable to reproduce.

The coexistence of both molecular islands and bare substrate (Figure 6A) suggests the film is only one molecule high, given that adsorption onto the substrate is typically more favorable than multilayer formation. The presence of vacancies in the film is further indication of the existence of only a single layer of HBC molecules. These data are strong evidence that the HBC deposits on the HOPG surface as a monolayer. We believe that this indicates the HBC to be predominately present in TCB as individual molecules under these conditions. Although it is impossible to conclusively rule out that HBC is actually dispersed as small aggregates which disassemble on the surface to give a monolayer, our STM data are in line with the spectroscopic observations, strongly suggesting that HBC is primarily dissolved in TCB as individual molecules. With this in mind, the positions of the three solvents in Figure 5B may yield

some information as to why only deposition from TCB was successful in forming an adsorbed HBC monolayer. TCB is highlighted in the top right of the graph, and is thus a “good” solvent ($(A_{355}/A_{421})_{\text{Ind}} = 4.10$), while 2-BOEA and CHB are in the lower left and therefore are “bad” solvents ($(A_{355}/A_{421})_{\text{Ind}} = 1.36$ and 1.98, respectively). One could infer that the presence of dispersed *monomeric* HBC is an important requirement for the formation of a monolayer, but further support for this conclusion is required. Similarly, the negative results from 2-BOEA and CHB depositions, although not conclusive on their own, seem to support the spectroscopic evidence of their inability to exfoliate HBC monomers.

Transmission Electron Microscopy of Exfoliated HBC.

The ultimate proof that HBC can be exfoliated down to individual molecules in good solvents would be to unambiguously image individual molecules using some form of microscopy. As described above; however, deposition of molecules from solution will result in self-assembled monolayer formation with perhaps a small minority of deposited molecules remaining as individuals. While it is undoubtedly possible to image such individual molecules on surfaces with STM or atomic force microscopy (AFM),^{56,57} such techniques are not well suited to searching large areas to find isolated, individual molecules. Conversely, transmission electron microscopy (TEM) is much more suitable for searching over large areas and has previously been used to image individual molecules.⁵⁸ However, we note that such imaging of small organic molecules has only been achieved by immobilizing them in structures such as carbon nanotubes,⁵⁸ or depositing them onto extremely well-defined surfaces such as graphene.⁵⁹ Nevertheless, we believe the relatively large size of HBC and its graphitic nature should facilitate its observation, if deposited on appropriate substrates. To facilitate the imaging of individual HBC molecules, we used a combination of aberration-corrected HRTEM and aberration-corrected scanning TEM (STEM).

Dilute dispersions of HBC in CHP were first deposited on ultrathin amorphous carbon supports. Shown in Figure 7A is a typical aberration-corrected HRTEM image of such a sample. This image shows a number of ordered regions with six-fold symmetry (see inset for FFT). These regions are typically ~ 5 nm in lateral size. We believe them to be ordered self-assembled layers of HBC molecules similar to those observed by STM (Figure 6). However, from time to time, very small 6-fold symmetric structures are observed as indicated by the white oval in Figure 7B. We believe this object to be a molecular aggregate consisting of two HBC molecules in an edge to edge arrangement. However, it is worth noting that the signal-to-noise ratio is extremely good. This means that we must consider the possibility that the aggregate may not be a single molecule thick but may in fact consist of an edge to edge aggregate of two pairs of cofacially stacked molecules.

We also deposited a dilute dispersion of HBC in CHP onto a very thin, solvent exfoliated, hexagonal boron nitride (h-BN) sheet.⁵¹ This was imaged using aberration-corrected, high angle annular dark field (HAADF) STEM. Shown in Figure 7C is a typical image obtained from this sample. This image clearly shows a region of approximately $1 \text{ nm} \times 1 \text{ nm}$ in extent with intensity different to the rest of the image (light colored region in the white box). The FFT corresponding to this region is shown as an inset. While the hexagonal structure in this FFT is clearly dominated by the h-BN lattice, it is worth noticing the absence of any amorphous contribution which would have appeared as an underlying ring in the FFT. This suggests that

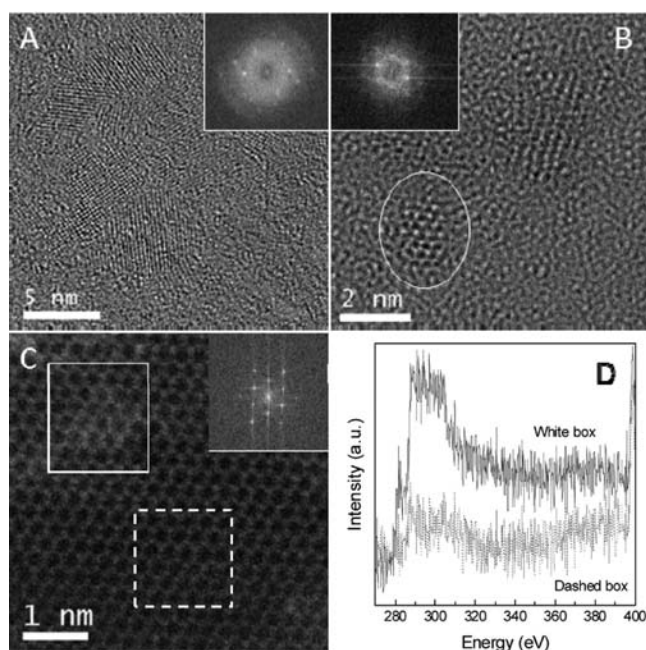


Figure 7. Transmission electron microscopy analysis of HBC deposited from CHP solution. (A) High resolution TEM image of self-assembled layers of HBC molecules in edge to edge arrangement. Inset: fast Fourier transform (FFT). (B) Isolated molecular edge-to-edge aggregate consisting of 2–6 molecules. Inset: FFT. (C) Scanning TEM image of a stacked molecular aggregate (white box). This aggregate consists of 1, 2, or 3 stacked molecules. (D) Electron energy loss spectra taken from the regions in panel C outlined by the white box and the dashed box.

the light colored region in the white box is fully crystalline and cannot be associated with contaminants lying on the h-BN substrate.

To show this region to be carbon-based, we performed electron energy loss spectroscopy (EELS) analysis on the area defined by the white box and compared it to an arbitrary region of surface (dashed box). The analysis of the core-loss carbon K-edge is shown in Figure 7D. While a carbon signal could be detected in the white box, no carbon was detected in the dashed box. In addition, a carbon K-edge signal could not be detected anywhere nearby on the h-BN flake, confirming the absence of any carbon contaminant whose signal would have caused image misinterpretation. Taken together, this shows the light colored region to be a crystalline, carbon-based structure. In addition, this region is very similar in shape and size to a HBC molecule. While it is impossible to definitively confirm from these images that this object is an individual HBC molecule, we believe this data strongly suggest this structure to be an individual molecule or very small cofacially stacked HBC aggregate. We note that analysis of the image intensities suggests that if it is not an individual molecule, it is a stack of no more than three HBC molecules.

CONCLUSIONS

In this work, we have demonstrated the first reported exfoliation of hexabenzocoronene in a large number of organic solvents. HBC was found to behave similarly to SWNTs, graphene, and fullerenes, with both halogenated solvents and amides being identified as successful dispersants. This suggests that solvation effects are dominated by HBC–solvent interactions in the basal plane rather than at the hydrogen-

terminated edge. Successful solvents are characterized by Hildebrand solubility parameters close to $21 \text{ MPa}^{1/2}$. However, even in the best solvents, considerable concentration-dependent aggregation effects are observed. We observe spectroscopic fingerprints of aggregation which can be used as metrics to quantify the aggregation state. By comparing such metrics at a common concentration, we can compare the ability of different solvents to exfoliate HBC to single molecules. We find a correlation between dispersed concentrations and exfoliation state, with cyclohexyl pyrrolidone, 1-bromonaphthalene, 1-chloronaphthalene, and 1,2,4-trichlorobenzene performing particularly well in both. STM measurements further substantiate these observations showing that, in selected cases, a “good” solvent such as 1,2,4-trichlorobenzene is able to induce the formation of ordered monolayer HBC films at the solid/liquid interface. Aberration corrected TEM can also be used to image self-assembled films of HBC when deposited from good solvents such as CHP. Occasionally, very small objects can also be found which have the characteristics of very small molecular aggregates or even individual molecules. Taken together we believe that this is strong evidence that HBC molecules exist as individuals in good solvents at low concentrations.

Finally, the fact that the solvent dependence of HBC dispersibility is so similar to that of graphene and carbon nanotubes suggests that previous studies on the dispersibility of these materials measured concentrations which were limited by solvent–solute interactions rather than sonication effects. This implies that the dispersion mechanisms for small graphitic molecules (HBCs) and large graphene nanosheets are identical, and hence that the solvents described here can be employed to disperse and exfoliate a range of graphitic molecules or nanomaterials over a broad set of length-scales. We note that the halogenated aromatic solvents show excellent performance in exfoliating and dispersing HBC. These have not been studied as possible solvents for graphene. We suggest that this might be a fruitful avenue for future research.

We predict that this work will allow the dispersion of unsubstituted versions of various recently synthesized planar and linear graphene-like molecules,^{7,60} facilitating a number of electronic applications. For example, preparation of hetero-junction solar cells from unfunctionalized HBC molecules¹⁴ should result in enhanced performance due to improved packing and more efficient space filling by the electro-active moieties. The ability to disperse graphitic molecules will be of particular relevance for graphene nanoribbons.^{30,61} These structures resemble linear arrays of HBC molecules and are expected to combine the properties of graphene with those of organic semiconductors resulting in transistors with high mobility and on–off ratio.⁶¹ It is widely believed that these structures will be important as the form of graphene most suited to use as nanoscale electronic devices. As such, the ability to process them will be critically important. This work provides the framework to approach the dispersion and deposition of such novel nanostructures.

EXPERIMENTAL METHODS

Hexabenzocoronene was dispersed in a range of solvents, divided into three broad categories: common lab solvents, amides and related solvents, and halogenated aromatic solvents. The solvents used were as follows: common lab solvents: tetrahydrofuran (THF), toluene, 2-butoxyethylacetate (2-BOEA), 2-nitropropane, ethyl acetate, methyl benzoate (MB), benzyl benzoate (BB), cyclohexylbenzene (CHB);

amide solvents: cyclohexyl pyrrolidone (CHP), *n*-methyl pyrrolidone (NMP), *n*-octyl pyrrolidone (N8P), *n*-dodecyl pyrrolidone (N12P), γ -butyrolactone (GBL), dimethylacetamide (DMA), *n*-ethyl pyrrolidone (NEP), *n*-benzyl pyrrolidone (NBenP), 1,3-dimethyl-2-imidazolidinone (DMEU), *n*-formylpiperidine (NFP), 1,3-dimethyl-3,4,5,6-tetrahydro-2(1H)-pyrimidinone (DMPU); halogenated aromatic solvents: 1,2,4-trichlorobenzene (TCB), 1,2-dichlorobenzene (DCB), 1-chloronaphthalene (1-CN), 1-bromonaphthalene (1-BN), fluorobenzene, bromobenzene, 4-chloroanisole, 2-bromoanisole, and 2-chlorophenol. We note that the acronyms introduced above will be used throughout the paper. Hildebrand and Hansen parameters were taken from the literature.⁴¹ All dispersions were prepared using a Branson 1510 sonic bath with quoted frequency of 42 kHz and power output of 80 W. We justify using bath sonication as it has previously been used to disperse and exfoliate graphene at high concentrations,²⁵ suggesting it should be appropriate for HBC dispersion. Another advantage of bath sonication is that its low power is unlikely to result in solvent degradation for the halogenated solvents, for example DCB and TCB. It is also extremely unlikely that such low-power sonication would result in degradation of the HBC. This is evidenced by the similarity between our measured absorption spectra (for highly exfoliated dispersions) and those reported for gas phase HBC molecules.^{2,35} In the initial phase of the experiment, solvent was added to between 1.5 and 2.0 mg of HBC at a concentration of 1 mg/mL in a 10 mL capacity vial which was then sonicated for 3 h. Samples were left to settle overnight and then centrifuged in 1.5 mL Eppendorf vials at a speed of 13 000 rpm ($\sim 16 400g$) for 15 min to remove any undispersed material. Any subsequent variations on this sample preparation method are described in the text.

Absorption spectra were taken over the wavelength range 300–900 nm (except where solvent absorbance interfered) using either a 2 mm or 1 mm quartz cuvette in a Cary 6000i UV–vis–NIR spectrophotometer. Photoluminescence spectra (excitation and emission scans and excitation–emission maps) were measured using a Cary Eclipse fluorescence spectrometer, in either a 1 cm \times 1 cm or 2 mm \times 2 mm quartz cuvette. In particular, the excitation wavelength for the emission scans was determined by the position of the maximum absorption in the UV–vis spectrum (typically, ~ 355 nm), with the emission data acquired between 370 and 650 nm, except where specified. Excitation spectra then had an emission wavelength defined by the position of the maximum emission (generally, ~ 484 nm), with the excitation spectrum typically collected from 250 to ~ 470 nm. Excitation–emission maps had an excitation range of 320–420 nm and an emission range of 440–620 nm.

All STM measurements were performed using a Veeco STM with a Nanoscope E controller equipped with an A-type scanner, using mechanically sheared Pt/Ir tips. The HBC dispersions were briefly sonicated prior to deposition. A droplet of dispersion was placed onto a highly oriented pyrolytic graphite (HOPG) surface and imaging was performed in the droplet. Prior to deposition, the HOPG surface was cleaned by stripping the top HOPG layers using Scotch tape. The tunnelling bias voltage was applied to the sample so that, for example, negative biases refer to filled state imaging. Typical values of the tunnelling bias and current were in the range -1.1 to $+0.7$ V and 100 to 700 pA, respectively. Drift correction and calibration with respect to the graphitic atomic lattice were performed on images where the tunnelling parameters had been switched halfway through so as to have HBC molecular resolution in the upper half and HOPG atomic resolution in the lower half of the image. The WSxM software⁶² was used to analyze and process the STM data.

For aberration corrected HRTEM a dispersion of HBC in CHP was drop-cast onto an ultrathin carbon support on a copper TEM grid (Agar Scientific, S186-4). The specimen was then imaged using the Oxford-JEOL 2200MCO FEG(S)TEM, fitted with two CEOS Cs aberration correctors, operated at 80 kV. For aberration-corrected STEM and EELS a dispersion of HBC in CHP was drop-cast onto hexagonal BN flakes, which had been exfoliated⁵¹ and deposited from the liquid phase onto a holey carbon TEM grid. The specimen was then imaged using a Nion UltraSTEM 100 operated at 60 kV. In both cases, to avoid contamination due to the presence of residual,

unevaporated solvent, the specimens were gently baked at 50 °C in vacuum overnight.

■ ASSOCIATED CONTENT

■ Supporting Information

Detailed description of aggregation metrics and analysis in terms of Hansen solubility parameters. This material is available free of charge via the Internet at <http://pubs.acs.org>.

■ AUTHOR INFORMATION

Corresponding Author

colemaj@tcd.ie

Notes

The authors declare no competing financial interest.

■ ACKNOWLEDGMENTS

J.N.C. would like to acknowledge the Science Foundation Ireland (Grant Number 07/IN.7/11772) for financial support.

■ REFERENCES

- (1) Clar, E.; Ironside, C. T.; Zander, M. *J. Chem. Soc. (Resumed)* **1959**, 142.
- (2) Kokkin, D. L.; Troy, T. P.; Nakajima, M.; Nauta, K.; Varberg, T. D.; Metha, G. F.; Lucas, N. T.; Schmidt, T. W. *Astrophys. J.* **2008**, *681*, L49.
- (3) Natsume, Y.; Minakata, T.; Aoyagi, T. *Thin Solid Films* **2009**, *517*, 3005.
- (4) Steglich, M.; Bouwman, J.; Huisken, F.; Henning, T. *Astrophys. J.* **2011**, *742*, 2.
- (5) Wong, W. W. H.; Singh, T. B.; Vak, D.; Pisula, W.; Yan, C.; Feng, X. L.; Williams, E. L.; Chan, K. L.; Mao, Q. H.; Jones, D. J.; Ma, C. Q.; Mullen, K.; Bauerle, P.; Holmes, A. B. *Adv. Funct. Mater.* **2010**, *20*, 927.
- (6) Wu, J.; Pisula, W.; Muellen, K. *Chem. Rev.* **2007**, *107*, 718.
- (7) Rouhanipour, A.; Roy, M.; Feng, X. L.; Rader, H. J.; Mullen, K. *Angew. Chem., Int. Ed.* **2009**, *48*, 4602.
- (8) Simpson, C. D.; Brand, J. D.; Berresheim, A. J.; Przybilla, L.; Rader, H. J.; Mullen, K. *Chem.—Eur. J.* **2002**, *8*, 1424.
- (9) Fleming, A. J.; Coleman, J. N.; Dalton, A. B.; Fechtenkoetter, A.; Watson, M. D.; Muellen, K.; Byrne, H. J.; Blau, W. J. *J. Phys. Chem. B* **2003**, *107*, 37.
- (10) Kastler, M.; Pisula, W.; Wasserfallen, D.; Pakula, T.; Mullen, K. *J. Am. Chem. Soc.* **2005**, *127*, 4286.
- (11) van de Craats, A. M.; Stutzmann, N.; Bunk, O.; Nielsen, M. M.; Watson, M.; Mullen, K.; Chanzy, H. D.; Sirringhaus, H.; Friend, R. H. *Adv. Mater.* **2003**, *15*, 495.
- (12) van de Craats, A. M.; Warman, J. M. *Adv. Mater.* **2001**, *13*, 130.
- (13) Wong, W. W. H.; Jones, D. J.; Yan, C.; Watkins, S. E.; King, S.; Haque, S. A.; Wen, X.; Ghiggino, K. P.; Holmes, A. B. *Org. Lett.* **2009**, *11*, 975.
- (14) Schmidt-Mende, L.; Fechtenkoetter, A.; Mullen, K.; Moons, E.; Friend, R. H.; MacKenzie, J. D. *Science* **2001**, *293*, 1119.
- (15) Englert, J. M.; Hauke, F.; Feng, X.; Muellen, K.; Hirsch, A. *Chem. Commun.* **2010**, *46*, 9194.
- (16) Hendel, W.; Khan, Z. H.; Schmidt, W. *Tetrahedron* **1986**, *42*, 1127.
- (17) Geim, A. K. *Science* **2009**, *324*, 1530.
- (18) Novoselov, K. S.; Geim, A. K.; Morozov, S. V.; Jiang, D.; Zhang, Y.; Dubonos, S. V.; Grigorieva, I. V.; Firsov, A. A. *Science* **2004**, *306*, 666.
- (19) Novoselov, K. S.; Jiang, D.; Schedin, F.; Booth, T. J.; Khotkevich, V. V.; Morozov, S. V.; Geim, A. K. *Proc. Natl. Acad. Sci. U.S.A.* **2005**, *102*, 10451.
- (20) Blake, P.; Brimicombe, P. D.; Nair, R. R.; Booth, T. J.; Jiang, D.; Schedin, F.; Ponomarenko, L. A.; Morozov, S. V.; Gleeson, H. F.; Hill, E. W.; Geim, A. K.; Novoselov, K. S. *Nano Lett.* **2008**, *8*, 1704.
- (21) Bourlinos, A. B.; Georgakilas, V.; Zboril, R.; Steriotis, T. A.; Stubos, A. K. *Small* **2009**, *5*, 1841.
- (22) Hamilton, C. E.; Lomeda, J. R.; Sun, Z.; Tour, J. M.; Barron, A. R. *Nano Lett.* **2009**, *9*, 3460.
- (23) Hernandez, Y.; Lotya, M.; Rickard, D.; Bergin, S. D.; Coleman, J. N. *Langmuir* **2010**, *26*, 3208.
- (24) Hernandez, Y.; Nicolosi, V.; Lotya, M.; Blighe, F. M.; Sun, Z.; De, S.; McGovern, I. T.; Holland, B.; Byrne, M.; Gun'Ko, Y. K.; Boland, J. J.; Niraj, N. P. P.; Duesberg, G.; Krishnamurthy, S.; Goodhue, R.; Hutchison, J.; Scardaci, V.; Ferrari, A. C.; Coleman, J. N. *Nat. Nanotechnol.* **2008**, *3*, 563.
- (25) Khan, U.; O'Neill, A.; Lotya, M.; De, S.; Coleman, J. N. *Small* **2010**, *6*, 864.
- (26) O'Neill, A.; Khan, U.; Nirmalraj, P. N.; Boland, J.; Coleman, J. N. *J. Phys. Chem. C* **2011**, *115*, 5422.
- (27) Nuvoli, D.; Valentini, L.; Alzari, V.; Scognamiglio, S.; Bon, S. B.; Piccinini, M.; Illescas, J.; Mariani, A. *J. Mater. Chem.* **2011**, *21*, 3428.
- (28) Coleman, J. N. *Acc. Chem. Res.* **2012**, DOI: 10.1021/ar300009f.
- (29) Rieger, R.; Muellen, K. *J. Phys. Org. Chem.* **2010**, *23*, 315.
- (30) Cai, J. M.; Ruffieux, P.; Jaafar, R.; Bieri, M.; Braun, T.; Blankenburg, S.; Muoth, M.; Seitsonen, A. P.; Saleh, M.; Feng, X. L.; Mullen, K.; Fasel, R. *Nature* **2010**, *466*, 470.
- (31) Bergin, S. D.; Nicolosi, V.; Streich, P. V.; Giordani, S.; Sun, Z.; Windle, A. H.; Ryan, P.; Niraj, N. P. P.; Wang, Z. T. T.; Carpenter, L.; Blau, W. J.; Boland, J. J.; Hamilton, J. P.; Coleman, J. N. *Adv. Mater.* **2008**, *20*, 1876.
- (32) Ruoff, R. S.; Tse, D. S.; Malhotra, R.; Lorents, D. C. *J. Phys. Chem.* **1993**, *97*, 3379.
- (33) Bergin, S. D.; Sun, Z. Y.; Rickard, D.; Streich, P. V.; Hamilton, J. P.; Coleman, J. N. *ACS Nano* **2009**, *3*, 2340.
- (34) Wu, J.; Watson, M. D.; Tchegobotareva, N.; Wang, Z.; Muellen, K. *J. Org. Chem.* **2004**, *69*, 8194.
- (35) Rouille, G.; Steglich, M.; Huisken, F.; Henning, T.; Muellen, K. *J. Chem. Phys.* **2009**, *131*, 204311.
- (36) Rickard, D.; Giordani, S.; Blau, W.; Coleman, J. N. *J. Lumin.* **2008**, *128*, 31.
- (37) Wu, J. S.; Fechtenkoetter, A.; Gauss, J.; Watson, M. D.; Kastler, M.; Fechtenkoetter, C.; Wagner, M.; Mullen, K. *J. Am. Chem. Soc.* **2004**, *126*, 11311.
- (38) Tobe, Y.; Utsumi, N.; Kawabata, K.; Nagano, A.; Adachi, K.; Araki, S.; Sonoda, M.; Hirose, K.; Naemura, K. *J. Am. Chem. Soc.* **2002**, *124*, 5350.
- (39) Hildebrand, J. H.; Prausnitz, J. M.; Scott, R. L. *Regular and Related Solutions*; Van Nostrand Reinhold Company: New York, 1970.
- (40) Hughes, J. M.; Aherne, D.; Coleman, J. N. *J. Appl. Polym. Sci.* **2012**, DOI: 10.1002/app.38051.
- (41) Hansen, C. M. *Hansen Solubility Parameters—A User's Handbook*; CRC Press: Boca Raton, FL, 2007.
- (42) Hughes, J. M.; Aherne, D.; Bergin, S. D.; O'Neill, A.; Streich, P. V.; Hamilton, J. P.; Coleman, J. N. *Nanotechnology* **2012**, *23*, 265604.
- (43) Cataldo, F. *Fullerenes, Nanotubes, Carbon Nanostruct.* **2009**, *17*, 79.
- (44) Coleman, J. N. *Adv. Funct. Mater.* **2009**, *19*, 3680.
- (45) Kastler, M.; Pisula, W.; Wasserfallen, D.; Pakula, T.; Muellen, K. *J. Am. Chem. Soc.* **2005**, *127*, 4286.
- (46) Grell, M.; Bradley, D. D. C.; Long, X.; Chamberlain, T.; Inbasekaran, M.; Woo, E. P.; Soliman, M. *Acta Polym.* **1998**, *49*, 439.
- (47) Grell, M.; Bradley, D. D. C.; Ungar, G.; Hill, J.; Whitehead, K. S. *Macromolecules* **1999**, *32*, 5810.
- (48) Birks, J. B.; Braga, C. L.; Lumb, M. D. *Proc. R. Soc. A* **1965**, *283*, 83.
- (49) Birks, J. B.; Christophorou, L. G. *Nature* **1963**, *197*, 1064.
- (50) Birks, J. B. *Rep. Prog. Phys.* **1975**, *38*, 903.
- (51) Coleman, J. N.; Lotya, M.; O'Neill, A.; Bergin, S. D.; King, P. J.; Khan, U.; Young, K.; Gaucher, A.; De, S.; Smith, R. J.; Shvets, I. V.; Arora, S. K.; Stanton, G.; Kim, H. Y.; Lee, K.; Kim, G. T.; Duesberg, G. S.; Hallam, T.; Boland, J. J.; Wang, J. J.; Donegan, J. F.; Grunlan, J. C.; Moriarty, G.; Shmeliov, A.; Nicholls, R. J.; Perkins, J. M.; Grievson, E. M.; Theuwissen, K.; McComb, D. W.; Nellist, P. D.; Nicolosi, V. *Science* **2011**, *331*, 568.

- (52) Samori, P.; Severin, N.; Simpson, C. D.; Muellen, K.; Rabe, J. P. *J. Am. Chem. Soc.* **2002**, *124*, 9454.
- (53) De Feyter, S.; Gesquiere, A.; Abdel-Mottaleb, M. M.; Grim, P. C. M.; De Schryver, F. C.; Meiners, C.; Sieffert, M.; Valiyaveetil, S.; Mullen, K. *Acc. Chem. Res.* **2000**, *33*, 520.
- (54) Schmitz-Hubsch, T.; Sellam, F.; Staub, R.; Torker, M.; Fritz, T.; Kubel, C.; Mullen, K.; Leo, K. *Surf. Sci.* **2000**, *445*, 358.
- (55) Strohmaier, R.; Petersen, J.; Gompf, B.; Eisenmenger, W. *Surf. Sci.* **1998**, *418*, 91.
- (56) Gross, L. *Nat. Chem.* **2011**, *3*, 273.
- (57) Jung, T. A.; Schlittler, R. R.; Gimzewski, J. K. *Nature* **1997**, *386*, 696.
- (58) Koshino, M.; Tanaka, T.; Solin, N.; Suenaga, K.; Isobe, H.; Nakamura, E. *Science* **2007**, *316*, 853.
- (59) Schaffel, F.; Wilson, M.; Warner, J. H. *ACS Nano* **2011**, *5*, 9428.
- (60) Yang, X. Y.; Dou, X.; Rouhanipour, A.; Zhi, L. J.; Rader, H. J.; Mullen, K. *J. Am. Chem. Soc.* **2008**, *130*, 4216.
- (61) Li, X. L.; Wang, X. R.; Zhang, L.; Lee, S. W.; Dai, H. J. *Science* **2008**, *319*, 1229.
- (62) Horcas, I.; Fernandez, R.; Gomez-Rodriguez, J. M.; Colchero, J.; Gomez-Herrero, J.; Baro, A. M. *Rev. Sci. Instrum.* **2007**, *78*, 013705.